HHS Public Access

Author manuscript

Nature. Author manuscript; available in PMC 2010 July 21.

Published in final edited form as:

Nature. 2010 January 21; 463(7279): 379–383. doi:10.1038/nature08701.

Mechanism of Folding Chamber Closure in a Group II Chaperonin

Junjie Zhang[1,2], **Matthew L. Baker**[2], **Gunnar F. Schröder**[3,*], **Nicholai R. Douglas**[4], **Stefanie Reissmann**[4,**], **Joanita Jakana**[2], **Matthew Dougherty**[2], **Caroline J. Fu**[2], **Michael Levitt**[3], **Steven J. Ludtke**[1,2], **Judith Frydman**[4], and **Wah Chiu**[1,2]

[1]Graduate Program in Structural and Computational Biology and Molecular Biophysics, Baylor College of Medicine, Houston, TX 77030

[2]National Center for Macromolecular Imaging, Verna and Marrs McLean Department of Biochemistry and Molecular Biology, Baylor College of Medicine, Houston, TX 77030

[3]Department of Structural Biology, Stanford University, Stanford, CA 94305

[4]Department of Biology and BioX Program, Stanford University, Stanford, CA 94305

Abstract

Group II chaperonins are essential mediators of cellular protein folding in eukaryotes and archaea. These oligomeric protein machines, ~1MDa, consist of two back-to-back rings encompassing a central cavity that accommodates polypeptide substrates[1,2,3]. Chaperonin-mediated protein folding is critically dependent on the closure of a built-in lid[4,5], which is triggered by ATP hydrolysis[6]. The structural rearrangements and molecular events leading to lid closure are still unknown. Here, we report four single particle cryo-EM structures of Mm-cpn, an archaeal group II chaperonin[5,7], in the nucleotide-free (open) and nucleotide-induced (closed) states. The 4.3 Å resolution of the closed conformation allowed building of the first ever atomic model directly from the cryo-EM density map, in which we were able to visualize the nucleotide and over 70% of the sidechains. The model of the open conformation was obtained by using the deformable elastic network modeling with the 8 Å resolution open state cryo-EM density restraints. Together, the open and closed structures reveal how local conformational changes triggered by ATP hydrolysis lead to an alteration of intersubunit contacts within and across the rings, ultimately causing a

Correspondence and requests for materials should be addressed to W.C. (wah@bcm.edu)..

*Present address: Institut für Strukturbiologie und Biophysik (ISB-3), Forschungszentrum Jülich, 52425 Jülich, Germany

**Present address: Max-Planck-Institut fuer terrestrische Mikrobiologie, Karl-von-Frisch Strasse, 35043 Marburg, Germany

Author Contributions J.Z. and J.J. collected the cryo-EM image data. J.Z. performed the image processing and reconstructions with the assistance of C.J.F. M.L.B. did the modeling and analysis of the closed state. G.F.S. did the model fitting for the open state. N.R.D. and S.R. designed the lidless mutation, the biochemical conditions for the cryo-EM experiments and performed all biochemical characterizations and experiments. S.J.L. advised on data processing and map filtering. J.Z., N.R.D., M.L.B., G.F.S., J.F. and W.C. interpreted the structural results. M.D., W.C. and J.Z. prepared all the movies. All authors contributed to the preparation of the manuscript.

Author Information The 3-D cryo-EM density maps have been deposited into the EBIMSD EMD database with accession codes: EMD-5137 (wild-type closed), EMD-5138 (lidless closed), EMD-5139 (wild-type open) and EMD-5140 (lidless open). The atomic models have been deposited in the Protein Data Bank as 3IYE (wild-type closed) and 3IYF (lidless open).

Supplementary Information is linked to the online version of the paper at www.nature.com/nature.

Full Methods and any associated references are available in the online version of the paper at www.nature.com/nature.

rocking motion that closes the ring. Our analysis reveals an intricate and unforeseen set of interactions controlling allosteric communication and inter-ring signaling driving the conformational cycle of group II chaperonins. Beyond this, we anticipate our methodology of combining single particle cryo-EM and computational modeling will become a powerful tool in the determination of atomic details involved in the dynamic processes of macromolecular machines in solution.

Chaperone-mediated protein folding is critical for the survival and proper function of cells[8]. Impairment of this process has been implicated in a variety of diseases including neurodegeneration, heart disease and cancer[9]. The eukaryotic hetero-oligomeric chaperonin TRiC is a unique class of molecular chaperones that assist the folding of an essential subset of cellular proteins with complex topologies, including many cell cycle regulators and cytoskeletal proteins[10]. Recent work suggests that the eukaryotic chaperonin is a potent inhibitor of Huntingtin aggregation and toxicity[11],[12].

Chaperonins consist of two back-to-back rings with a total of 14 to 18 subunits. Each subunit is composed of three domains: an equatorial domain that binds ATP and provides inter-ring contacts, an apical domain which binds the substrate and an intermediate hinge domain[4],[13]. All chaperonins use ATP hydrolysis to drive a conformational cycle that encapsulates folding substrates within a central chamber[14],[15]. Based on the mechanism of encapsulation, chaperonins can be separated into two related, but distinct groups. Group I chaperonins, mostly found in bacteria and endosymbiotic organelles (such as GroEL), have a co-factor (GroES) serving as a detachable lid that binds the apical domains and closes the chamber. Group II chaperonins, found in archaea and eukaryotes, have a builtin lid segment protruding from each apical domain. The molecular mechanism of lid closure in group II chaperonins is virtually unknown, due in large measure to the lack of high resolution structures for the different states in the conformational cycle.

Here, we derive the structures of a group II chaperonin in both open (nucleotide-free) and closed (ATP-induced) states at unprecedented resolutions by single particle cryo-EM and computational modeling. Our analysis reveals that in group II chaperonins the key structural rearrangements leading from the open to closed state are completely different from those found in group I chaperonins, despite structural similarities between the groups.

The 16-mer homo-oligomeric chaperonin from the mesophilic archaea *Methanococcus maripaludis* (Mm-cpn) provides a simple and tractable model for understanding group II chaperonins[5],[7],[16]. Mm-cpn folds proteins in an ATP-dependent manner and shares the allosteric regulation properties of eukaryotic chaperonins such as TRiC[5],[7]. A variant of Mm-cpn lacking the built-in lid (herein termed “lidless Mm-cpn”) can still bind unfolded polypeptides and hydrolyze ATP, but is unable to mediate folding of a stringent substrate[5]. Because the structural analysis of the nucleotide-free state was dominated by end-on views of the wild-type particles on an electron microscope grid, likely due to the exposed hydrophobic interior of the open lid, we used lidless Mm-cpn (which has random orientations on the EM grid) for the cryo-EM structural investigation of the poorly understood open state of group II chaperonins.

2-D averages of cryo-EM images of wild-type and lidless Mm-cpn show they transition uniformly from an open, nucleotide free state to a closed conformation upon incubation with ATP/AlFx (Supplement Fig. 1). These observations contrast to previous findings[17], and suggest that ATP hydrolysis may yield a defined 3-D conformation of Mm-cpn, as observed in the eukaryotic chaperonin TRiC[6],[15], thus making high resolution structural determination tractable.

Fig. 1a shows the 4.3 and 4.8 Å resolution reconstructions of the wild-type and lidless Mm-cpn in the ATP-induced closed state, respectively (Supplement Fig. 2e). Both wild-type and lidless Mm-cpn achieved essentially the same closed structure (Fig. 1a). The resolution of the wild-type closed-state map is sufficient to permit unambiguous segmentation of the density of each subunit (Supplement Movie 1) as well as the modeling of the Mm-cpn subunits from residues 1 to 532 (Fig. 1b, Supplement Movie 2). The α-helix pitch and β-strand separation are clearly visible in the density map, as expected at this resolution[18] (Supplement Fig. 3). Strikingly, more than 70% of sidechain densities are visible in the map with more than a quarter of the sidechain densities (143 out of 532) fully visible (Fig. 1c, Supplement Fig. 4, Supplement Movie 3). These features allowed for the construction of the first atomic model built directly from the cryo-EM density without the aid of a crystal, a feat not yet carried out in previous near-atomic resolution single particle cryo-EM studies[19],[20],[21],[22]. Additionally, density likely representing nucleotide in the ATP-binding pocket is also seen in close contact with α-helices A, B, D, F, L and the end of the "stem-loop" [4] (Fig. 1d).

In the absence of nucleotide, both chaperonin variants were uniformly open (Fig. 2a, Supplement Fig. 1). An 8 Å resolution map of Mm-cpn open state was reconstructed from images of nucleotide-free lidless Mm-cpn. The resolution of this open-state map is likely limited by the structural flexibility of the chaperonin (Supplement Movie 4). The flexibility appears highest in the apical domain, as illustrated in the lidless Mm-cpn map where the α-helices are well resolved in the equatorial domain (Fig. 2b) but less resolved in the apical and intermediate domains. This resonates with the structural analysis of Group I chaperonins, as the apical domain residues in GroEL crystals have higher B-factors[23], and may reflect the dynamic nature of the substrate binding sites. In the wild-type Mm-cpn, the open lid tends to cause the chaperonins to orient preferentially with mostly end-on views, accounting for anisotropic sampling of the data and thus a lower resolution reconstruction of 10 Å (Supplement Fig. 2e) as shown in other study[24].

As in the closed state, the maps of the lidless and wild-type open-state Mm-cpn are very similar (Fig. 2a) indicating that the presence of the lid does not significantly affect the open conformation. Due to the clear visibility of secondary structure elements in the 8 Å lidless open-state map, a model for the open-state subunit (Fig. 2c) was built based on the closed-state model and a geometry-constrained, deformable elastic network modeling approach[25] (see Methods).

Given that wild-type and lidless Mm-cpn subunits essentially adopt the same structures for both the open and closed states, we used the models built from the highest resolution maps of the open and closed Mm-cpn states to gain insight into key structural changes

accompanying ATP hydrolysis in group II chaperonins. Our analysis reveals that the intra- and inter-ring interactions change dramatically between the open and closed states.

In the closed state, adjacent subunits within a ring engage in extensive interactions throughout all three domains (Fig. 3a, right). In contrast, neighboring subunits in the open state are connected primarily through interactions in the equatorial domain (Fig. 3a, left). This may account for the higher flexibility, and lower resolution, of the apical domains in the open state. One of the invariant intra-ring contacts observed in both open and closed states is between Asp45 and Arg511 in the adjacent subunits (Supplement Movie 5). An overlap of these models shows that every subunit within one ring rotates ~40° around this interface during the conformational transition from open to closed state, suggesting that the Asp45 and Arg511 residue pair serves as a hinge for intra-ring motion (Fig. 3a,b and Supplement Movie 5).

Another important component of intra-ring communication is a β-sheet formed between the stem-loop of one subunit and the N- and C-terminal segments of the neighboring subunit (Fig. 3b). Of note, our ability to visualize almost the entire N- and C-termini (except for the last 11 residues) in the closed state to a level of detail not observed in any previous chaperonin structures[4,13,26,27] uncovered a dramatic movement of these structural elements during the conformational change of group II chaperonins. In the open state, this β-sheet is tilted upwards, with the visible portions of the flexible N- and C-termini pointing towards the central chamber of Mm-cpn (Fig. 3a,b, left panels, Supplement Movie 5). By contrast, these residues are pushed downwards and retracted from the chamber in the closed state (Fig. 3a,b, right panels, Supplement Movie 5). As a result, the N- and C-termini become more rigid in the closed state, allowing for visualization and modeling of the complete N-terminus and nearly all of the C-terminus (up to Gly532, Fig. 3a,b right panel).

This structural rearrangement of the termini is supported by differential protease sensitivity observed for the C-terminus of lidless Mm-cpn in the open and closed states (Fig. 3c and Supplement Fig. 6). N-terminus is cleaved at Tyr15 in both open and closed states, consistent with our models, which predict Tyr15 to be at the N-terminal β-strand which is further away from the stem-loop (Fig. 3b). In contrast, the C-terminus is cleaved at several positions in the open state (bands indicated by * signs in Fig. 3c), but protected from proteolysis in the closed state, consistent with a highly flexible conformation of the C-terminal tail. The observed protection induced by hydrolysable ATP (Fig. 3a,b) is consistent with our structural conclusion that the C-terminal residues become more rigid in the ATP-induced state. These previously unseen movements of the N- and C-termini in and out of the chaperonin chamber may contribute to chaperonin mediated folding. Notably, the C-terminus of Mm-cpn contains a conserved GGM repeat that is also found in bacterial group I chaperonins[28]. It has been suggested that, in GroEL, these regions play a role in the substrate folding process[28,29]. Our results provide direct structural evidence for the active involvement of N- and C-termini in the chaperonin conformational cycle. This “hand-shaking” structural signature between the N- and C-termini in one subunit and the stem-loop in the neighboring subunit may indeed be the key communication between subunits within one ring during ATP hydrolysis (Supplement Movie 5).

The mode of inter-ring communication in group II chaperonins has remained elusive. Unlike Group I chaperonins, where the rings contact in a staggered subunit arrangement[13], all group II chaperonins have a subunit in one ring directly aligned with another subunit in the trans-ring, leading to fully symmetrical and heterologous contacts (Supplement Fig. 5). Thus, inter-ring communication must occur directly between each pair of contacting subunits across the rings. Our structural analysis reveals that the molecular interactions at the ring-ring interface change dramatically between the open and closed states (Fig. 4a). In the closed state, the N- and C-termini of adjacent subunits across the ring are in close proximity (Fig. 4a,c, Supplement Movie 5), while helices M and O' on the exterior side of the inter-ring interface appear relatively distant. Surprisingly, these contacts change dramatically in the open state, with helices M and N in one subunit coming close to helix O' of the neighboring subunit across the ring. Our structures suggest that the open state is stabilized by a network of complementary charges linking Arg425 and Glu420 in Helices M and N with Asp451, Glu454, Lys458, Arg460 in Helix O' (Fig. 4b). The open state also causes a significant motion that separates the N- and C- termini from the subunits across the rings thereby pushing the termini towards the respective central chambers (Fig. 4a,c, Supplement Movie 5). Such a conformational switch of the termini also makes them more susceptible to protease digestion in the open state (Fig. 3c).

This analysis indicates that transition between the open and closed states in group II chaperonins involves a rocking motion that dramatically rearranges the inter-ring contacts. This movement differs radically from that observed in group I chaperonins[26]. This difference in inter-ring communication could result from the in-register ring-ring arrangement of group II chaperonins (Supplement Fig. 5), which allows greater freedom of tilting for the equatorial domains compared to the arrangement in GroEL. The staggered arrangement of inter-ring subunits in group I chaperonins leads to the relative conservation of inter-ring contacts throughout the conformational cycle. This quaternary structural feature in group II chaperonins may compensate for the lack of a lid-like GroES co-chaperonin and allow self-closure of the folding chamber through subunit rocking mediated by equatorial domain rotation.

A major question in understanding nanomachines driven by ATP hydrolysis is how local changes in the nucleotide binding site are communicated globally throughout the protein. The previous structures of group II chaperonins[15],[17],[24] did not reveal how ATP hydrolysis affects intra- and inter-ring communication. Our ability to identify how secondary structure elements move in response to ATP hydrolysis, allows us to hypothesize how local changes in the nucleotide-binding site can be propagated within and between rings. Our maps clearly indicate that helix L in the intermediate domain tilts in response to ATP hydrolysis (Fig. 4d). As a result, the distal C-terminal end of helix L moves towards the stem-loop. Concurrently, a concerted movement of contiguous helices L, M and N causes M and N to be farther away from the O' helix of the subunit across the ring (Fig. 4a,b). Together, these molecular events produce the forward rocking of the equatorial domain towards the center of the cavity, which is transmitted through the intermediate domain to the apical domain, thus closing the lid[15]. The effect of ATP hydrolysis on helix L and this stem-loop fits with the observation that D386 in helix L and D60 at the end of the stem-loop both contact the γ-phosphate mimic AlFx in the closed thermosome crystal structure[4] (Fig. 4d).

Our single particle cryo-EM analysis of Mm-cpn has revealed unprecedented detail of the open and closed states of group II chaperonins. The structural rearrangements observed here are strikingly different from those occurring in the well-studied group I chaperonins[26], indicating that a completely different mechanism of inter-subunit communication drives the folding cycles in group II chaperonins.

METHODS SUMMARY

Wild-type and lidless Mm-cpn were expressed and purified from E. coli[5]. Specimens were prepared for the cryo-EM experiments by rapid freezing using the Vitrobot (FEI, Hillsboro, OR). All imaging was done on a JEM3200FSC electron microscope (JEOL, Tokyo, Japan) with an in-column energy filter except for the wild-type open state which was imaged on a JEM2010F electron microscope. All data was recorded with Gatan 4k x4k CCD cameras (model #895, Pleasanton, CA). The particle images were processed using the standard EMAN procedures[30] with D8 symmetry imposed. The resolution of the reconstruction was assessed using the 0.5 Fourier Shell Correlation criterion. The number of particles used for 3-D reconstruction for wild-type closed, lidless closed, wild-type open and lidless open states were 29,926, 24,434, 27,598 and 18,168 respectively. The starting models for the Mm-cpn open and closed states were built from its homolog thermosome KS-1 (PDB ID: 1Q3Q). Model for the closed state was hand-built by crystallographic model building tool (see Full Methods). Model for the open state was refined with a deformable elastic network algorithm using DireX[25].

METHODS

Mm-cpn purification and cryo-specimen preparation

Both wild-type and lidless Mm-cpn were purified in the buffer (20 mM Hepes pH 7.4, 50 mM NaCl, 5 mM MgCl, 0.1 mM EDTA, 1 mM DTT, 10 % glycerol, 0.1 mM PMSF). They were then diluted in the ATPase buffer (20 mM TRis/HCl pH 7.5, 100 mM KCl, 5 mM MgCl, 1 mM DTT) to lower the glycerol concentration. 0.05% detergent OG was added to the open state of wild-type Mm-cpn buffer before cryo-EM freezing to yield more side views.

For the nucleotide-induced states of wild-type and lidless Mm-cpn, a 1 mM final concentration of ATP/AlFx was used. The sample was then incubated in a water bath at 37 °C for 1 hour before freezing onto the grid. This nucleotide concentration is high enough to overcome the negative cooperativity of ATP hydrolysis between two rings[5], thus, obtaining a more homogeneous closed-state Mm-cpn for high resolution structure determination. The nucleotide free Mm-cpn was incubated at 37 °C for 10 minutes before freezing onto the grid.

Samples were embedded in vitreous ice as follows. A 2.5 μL aliquot of the above-prepared samples was applied onto a 400-mesh R1.2/1.3 Quantifoil grid (Quantifoil Micro Tools GmbH, Jena Germany). The grid was previously washed and glow discharged. After applying the sample, the grid was blotted and rapidly frozen in liquid ethane using a Vitrobot (FEI, Hillsboro, OR) and stored in liquid nitrogen before imaging.

Proteinase K protection assay

Mm-Cpn was incubated with proteinase K as previously described, with slight modifications[5]. To generate AlFx, $Al(NO_3)_3$ (1mM) and NaF (6mM) were added to the reaction, then incubated at 37°C for 10 minutes. The chaperonin was incubated with 20 μg ml^{-1} proteinase K for 5 minutes at 25°C, then PMSF (5mM) was added to inhibit the proteinase K activity. Upon completion of the digestion, the reactions were placed on ice for 5 minutes, then analyzed by SDS-PAGE.

Cryo-EM data collection

The lidless Mm-cpn open and closed states and the wild-type Mm-cpn closed state were imaged on JEM3200FSC electron cryo-microscope operated at 300kV while the wild-type open state was imaged on JEM2010F electron microscope at 200 kV (JEOL Inc, Tokyo, Japan). Both microscopes have a field emission gun. Images from JEM3200FSC and JEM2010F were recorded at a detector magnification of 112,000 X and 83,100 X respectively on Gatan 4K×4K CCD cameras (model #895, Gatan, Pleasanton, CA). For the JEM3200FSC data collection, an in-column omega energy filter was used with a slit width of 10 eV. The particle images for the 4.3 Å resolution map of the wild-type closed state were obtained from 616 CCD frames using 2 grids with a defocus range of 1–2.5 μm.

Cryo-EM data processing

All the particle images were boxed out automatically using EMAN[30] program *batchboxer* and then manually screened using the EMAN program *boxer*. The class averages show that they are conformationally uniform (Supplement Fig. 1) in contrast to an earlier report showing multiple conformations in the apo state[17]. Contrast transfer functions (CTF) of these particles were first fitted using automatic CTF fitting program *fitctf.py*[31] and then manually examined and adjusted using the EMAN program *ctfit*.

All these particles were phase-flipped, and then an initial model of each of the four states was generated using the EMAN program *startcsym*. These four models were further refined against its 2-D image particles using the standard EMAN iterative reconstruction algorithm[30],[32] with D8 symmetry applied. The final resolutions of wild-type closed, lidless closed, wild-type open, lidless open states density maps were 4.3Å, 4.8 Å, 10 Å and 8 Å respectively according to the Fourier Shell Correlation[33] with 0.5 cut-off criterion (Supplementa Fig. 2e).

Cryo-EM map post-processing and visualization

The final density maps of the closed-state structures were filtered using the 1D structure factor curve calculated from their Cα models to enhance the high-resolution features and then Gaussian low-pass filtered to minimize the noise. Similar map-filtering techniques have been suggested earlier[34],[35]. Map segmentation, visualizations and animations are done in Chimera[36] and Amira (Visage Imaging™).

Closed-state model building

Initially, a homology model for Mm-cpn was constructed using thermosome KS-1 (PDB ID: 1Q3Q) as a template with Swiss-Model[37]. The Cα backbone of this model was then adjusted to fit the cryo-EM map density using Coot[38]. Secondary structure elements and protruding sidechain densities were used to anchor the Cα atoms in the model. Using EMAN, this model was then blurred to 4.5Å resolution, from which 1-D structure factor curve was calculated and used to scale the structure factor amplitudes of the density map. In this amplitude-scaled map, sidechain densities became more resolved and allowed for atomic modeling. We firstly focused on improving density fit for regions of secondary structure followed by sidechain fitting and loop modeling. During this process, we used a strategy similar to the crystallographic approach while modeling low-resolution X-ray structures: we optimized the proper geometry of the protein (bond length, bond angle, dihedral angle constraint, rotamer statistics). The dihedrals of the resulting model were assessed according to their positions in the Ramachandran plot using MolProbity[39]. To assess the map and model, we classified each amino acid into one of the four possible categories. “Fully-resolved” sidechains were termed as those where the local shape of the density matched well to the model sidechain rotamers. “Partially-resolved” sidechains had sidechains that fall within but not necessarily fit completely to an envelope of protruding density. “Ambiguous” sidechains had ambiguous fits of the Cα and sidechain atoms to the density. Glycines belong to the final category which has no sidechain. (Supplement Fig. 4)

Open-state model building

The open-state lidless Mm-cpn model was obtained by real-space refinement with the program DireX[25] using the homology model of the closed state as a starting model. DireX employs a geometry-based conformational sampling algorithm and the deformable elastic network (DEN) restraints plus the forces from the density map to maximize the correlation between the experimental density map and a density map computed from the model (see Supplement Methods).

The actual refinement for the open state Mm-cpn model was performed in two steps: First, strong non-deformable DEN restraints were used to obtain a fit with almost rigid subunits. In the second step, the DEN restraints were made weaker and deformable for flexibly refining the models. To account for missing experimental density in regions of high flexibility, residue-based B-factors were taken from the thermosome crystal structure (PDB ID: 1Q3Q), assigned to the homology model and used to scale the contribution of each residue to the model map. This reduced artificial structural distortions due to missing or significantly decreased density.

Supplementary Material

Refer to Web version on PubMed Central for supplementary material.

Acknowledgements

We acknowledge the support of grants from the National Institutes of Health through the Nanomedicine Development Center Roadmap Initiative, Biomedical Technology Research Center for Structural Biology in

National Center for Research Resources, Nanobiology Training Fellowship administered by the Keck Center of the Gulf Coast Consortia and the National Science Foundation.

REFERENCES

1. Bukau B, Horwich AL. The Hsp70 and Hsp60 chaperone machines. Cell. 1998; 92:351–366. [PubMed: 9476895]
2. Frydman J. Folding of newly translated proteins in vivo: the role of molecular chaperones. Annu Rev Biochem. 2001; 70:603–647. [PubMed: 11395418]
3. Hartl FU, Hayer-Hartl M. Molecular chaperones in the cytosol: from nascent chain to folded protein. Science. 2002; 295:1852–1858. [PubMed: 11884745]
4. Ditzel L, et al. Crystal structure of the thermosome, the archaeal chaperonin and homolog of CCT. Cell. 1998; 93:125–138. [PubMed: 9546398]
5. Reissmann S, Parnot C, Booth CR, Chiu W, Frydman J. Essential function of the built-in lid in the allosteric regulation of eukaryotic and archaeal chaperonins. Nat Struct Mol Biol. 2007; 14:432–440. [PubMed: 17460696]
6. Meyer AS, et al. Closing the folding chamber of the eukaryotic chaperonin requires the transition state of ATP hydrolysis. Cell. 2003; 113:369–381. [PubMed: 12732144]
7. Kusmierczyk AR, Martin J. Nucleotide-dependent protein folding in the type II chaperonin from the mesophilic archaeon Methanococcus maripaludis. Biochem J. 2003; 371:669–673. [PubMed: 12628000]
8. Dobson CM. Principles of protein folding, misfolding and aggregation. Semin Cell Dev Biol. 2004; 15:3–16. [PubMed: 15036202]
9. Balch WE, Morimoto RI, Dillin A, Kelly JW. Adapting proteostasis for disease intervention. Science. 2008; 319:916–919. [PubMed: 18276881]
10. Yam AY, et al. Defining the TRiC/CCT interactome links chaperonin function to stabilization of newly made proteins with complex topologies. Nat Struct Mol Biol. 2008; 15:1255–1262. [PubMed: 19011634]
11. Tam S, Geller R, Spiess C, Frydman J. The chaperonin TRiC controls polyglutamine aggregation and toxicity through subunit-specific interactions. Nat Cell Biol. 2006; 8:1155–1162. [PubMed: 16980959]
12. Kitamura A, et al. Cytosolic chaperonin prevents polyglutamine toxicity with altering the aggregation state. Nat Cell Biol. 2006; 8:1163–1170. [PubMed: 16980958]
13. Braig K, et al. The crystal structure of the bacterial chaperonin GroEL at 2.8 Å. Nature. 1994; 371:578–586. [PubMed: 7935790]
14. Saibil HR, et al. ATP induces large quaternary rearrangements in a cage-like chaperonin structure. Curr Biol. 1993; 3:265–273. [PubMed: 15335746]
15. Booth CR, et al. Mechanism of lid closure in the eukaryotic chaperonin TRiC/CCT. Nat Struct Mol Biol. 2008; 15:746–753. [PubMed: 18536725]
16. Kusmierczyk AR, Martin J. Nested cooperativity and salt dependence of the ATPase activity of the archaeal chaperonin Mm-cpn. FEBS Lett. 2003; 547:201–204. [PubMed: 12860414]
17. Clare DK, et al. Multiple States of a nucleotide-bound group 2 chaperonin. Structure. 2008; 16:528–534. [PubMed: 18400175]
18. Blow, D. Outline of Crystallography for Biologists. Oxford University Press; USA: 2002.
19. Ludtke SJ, et al. De novo backbone trace of GroEL from single particle electron cryomicroscopy. Structure. 2008; 16:441–448. [PubMed: 18334219]
20. Jiang W, et al. Backbone structure of the infectious epsilon15 virus capsid revealed by electron cryomicroscopy. Nature. 2008; 451:1130–1134. [PubMed: 18305544]
21. Zhang X, et al. Near-atomic resolution using electron cryomicroscopy and single-particle reconstruction. PNAS. 2008; 105:1867–1872. [PubMed: 18238898]
22. Yu X, Jin L, Zhou ZH. 3.88 Å structure of cytoplasmic polyhedrosis virus by cryo-electron microscopy. Nature. 2008; 453:415–419. [PubMed: 18449192]

23. Braig K, Adams PD, Brünger AT. Conformational variability in the refined structure of the chaperonin GroEL at 2.8 Å resolution. Nat Struct Biol. 1995; 2:1083–1094. [PubMed: 8846220]
24. Schoehn G, Hayes M, Cliff M, Clarke AR, Saibil HR. Domain rotations between open, closed and bullet-shaped forms of the thermosome, an archaeal chaperonin. J Mol Biol. 2000; 301:323–332. [PubMed: 10926512]
25. Schröder GF, Brunger AT, Levitt M. Combining efficient conformational sampling with a deformable elastic network model facilitates structure refinement at low resolution. Structure. 2007; 15:1630–1641. [PubMed: 18073112]
26. Xu Z, Horwich AL, Sigler PB. The crystal structure of the asymmetric GroEL-GroES-(ADP)7 chaperonin complex. Nature. 1997; 388:741–750. [PubMed: 9285585]
27. Boisvert DC, Wang J, Otwinowski Z, Horwich AL, Sigler PB. The 2.4 Å crystal structure of the bacterial chaperonin GroEL complexed with ATP gamma S. Nat Struct Biol. 1996; 3:170–177. [PubMed: 8564544]
28. Tang YC, et al. Structural features of the GroEL-GroES nano-cage required for rapid folding of encapsulated protein. Cell. 2006; 125:903–914. [PubMed: 16751100]
29. Suzuki M, et al. Effect of the C-terminal truncation on the functional cycle of chaperonin GroEL: implication that the C-terminal region facilitates the transition from the folding-arrested to the folding-competent state. J Biol Chem. 2008; 283:23931–23939. [PubMed: 18583344]
30. Ludtke SJ, Baldwin PR, Chiu W. EMAN: semiautomated software for high-resolution single-particle reconstructions. J Struct Biol. 1999; 128:82–97. [PubMed: 10600563]
31. Yang C, Jiang W, Cheng DH, Adiga U, Ng E, Chiu W. Estimating Contrast Transfer Function and Associated Parameters by Constrained Nonlinear Optimization. J Microsc. 2009; 233:391–403. [PubMed: 19250460]
32. Ludtke SJ, Jakana J, Song J-L, Chuang D, Chiu W. A 11.5 Å single particle reconstruction of GroEL using EMAN. J Mol Biol. 2001; 314:253–262. [PubMed: 11718559]
33. Harauz G, van Heel M. Exact filters for general geometry three dimensional reconstruction. Optik. 1986; 73:146–156.
34. Fernandez JJ, Luque D, Caston JR, Carrascosa JL. Sharpening high resolution information in single particle electron cryomicroscopy. J Struct Biol. 2008; 164:170–175. [PubMed: 18614378]
35. Rosenthal PB, Henderson R. Optimal determination of particle orientation, absolute hand, and contrast loss in single-particle electron cryomicroscopy. J Mol Biol. 2003; 333:721–745. [PubMed: 14568533]
36. Pettersen EF, et al. UCSF Chimera--a visualization system for exploratory research and analysis. J Comput Chem. 2004; 25:1605–1612. [PubMed: 15264254]
37. Arnold K, Bordoli L, Kopp J, Schwede T. The SWISS-MODEL workspace: a web-based environment for protein structure homology modelling. Bioinformatics. 2006; 22:195–201. [PubMed: 16301204]
38. Emsley P, Cowtan K. Coot: model-building tools for molecular graphics. Acta Crystallogr D Biol Crystallogr. 2004; 60:2126–2132. [PubMed: 15572765]
39. Lovell SC, et al. Structure validation by Calpha geometry: phi,psi and Cbeta deviation. Proteins. 2003; 50:437–450. [PubMed: 12557186]

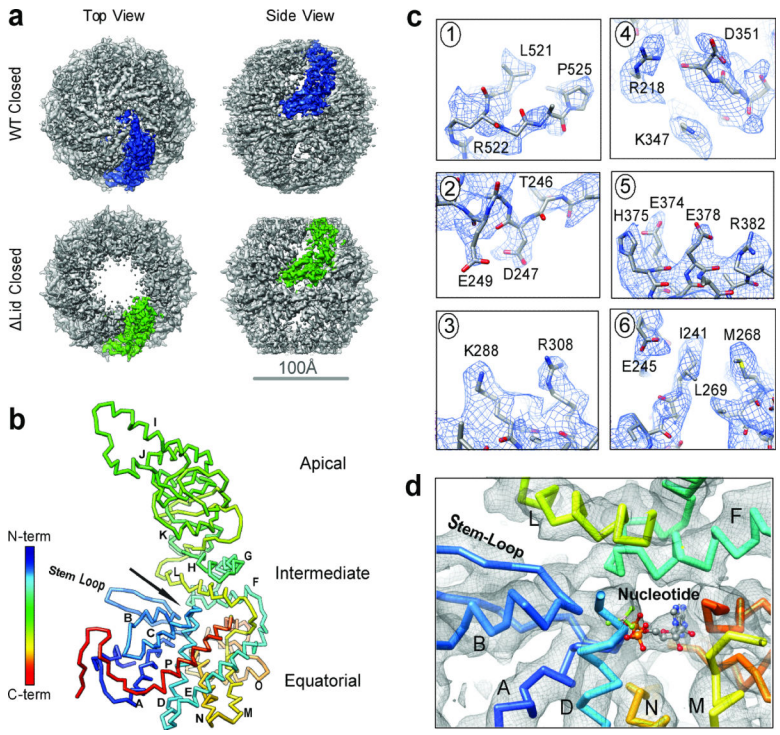

Figure 1. Cryo-EM structures of wild-type and lidless Mm-cpn in the closed state

a. Top and side views of the cryo-EM density maps with one subunit colored blue (wild-type) and green (lidless) at 4.3 and 4.8 Å resolution respectively.

b. Backbone model of the wild-type closed-state Mm-cpn subunit. The black arrow indicates the nucleotide-binding pocket. Helices are labeled from A to P.

c. Examples of visible sidechain densities (blue mesh) in the wild-type Mm-cpn map.

d. Map and backbone model around the nucleotide-binding pocket in **(b)**.

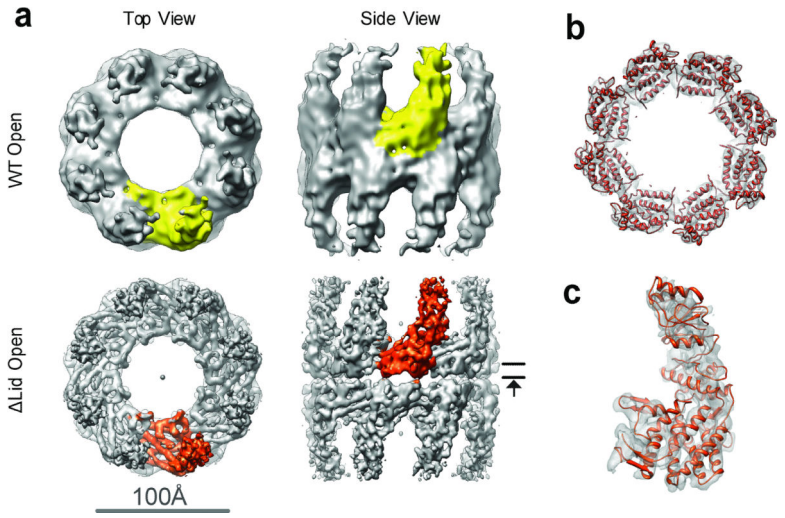

Figure 2. Cryo-EM structures of wild-type and lidless Mm-cpn in the open state

a. Top and side views of the Mm-cpn density maps with one subunit colored yellow (wild-type) and orange (lidless) at 10 and 8 Å resolution respectively.

b. Slice of density map in the equatorial domain of the lidless Mm-cpn open map with α-helices (orange ribbons) fitted into the density. The viewing direction is indicated by the arrow in (**a**).

c. Model of the lidless (orange) open-state Mm-cpn single subunit flexibly fitted into the cryo-EM density map.

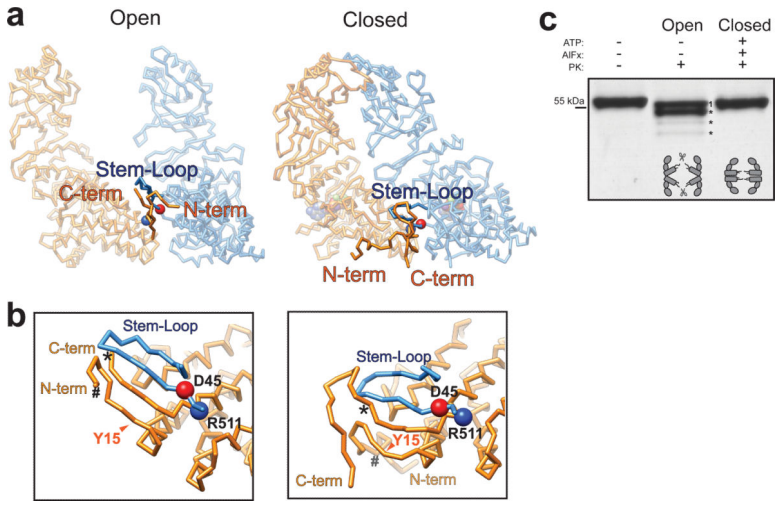

Figure 3. Molecular interactions of Mm-cpn subunits within one ring in two states

a. Backbone models for two neighboring subunits of two states viewed from the central cavity with nucleotides as sphere models.

b. Zoom-in regions of the stem-loop and N- and C-termini viewed from the right in **(a)**. (#) for Val7 and (*) for Glu519 which could be modeled in the open states.

c. SDS-PAGE gel of Protease K treatment of lidless Mm-cpn showing that residues 1–14 get cut for both states (band 1), and the C-terminus can be cut in multiple locations only for the open state (*).

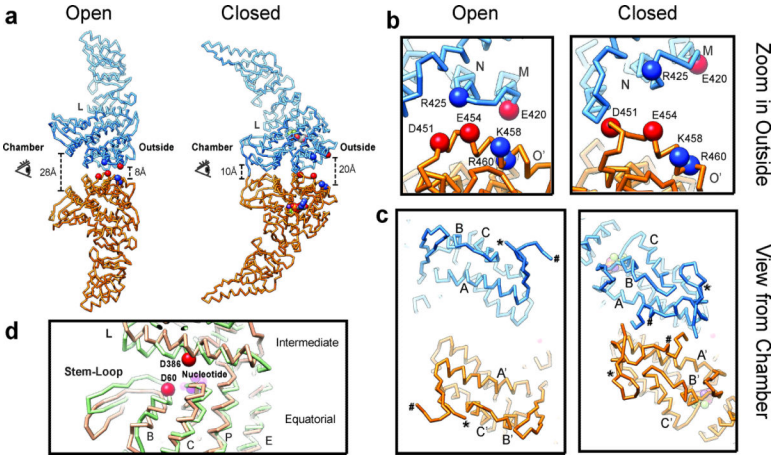

Figure 4. Molecular Interactions between Mm-cpn subunits across rings in two states and the conformational changes around the nucleotide binding pocket with some helices labeled

a. Backbone models for two adjacent subunits across the rings of two states.

b. Insets of the helix O region of two states with positively-charged (blue) and negatively-charged (red) residues as spheres.

c. Insets showing the N and C termini viewed by the “eyes” in (**a**). (#) and (*) have the same definitions as in Figure 3.

d. Aligned nucleotide binding pockets from the closed-state (green) and open-state (orange) models.